Chapter 5
Uncorrelated Noise Sources Separation Using Inverse Beamforming

Claudio Colangeli, Paolo Chiariotti, and Karl Janssens

Abstract The separation of a measured sound field in uncorrelated sources distributions can be very useful when dealing with sound source localization problems. The use of the Principal Component Analysis (PCA) principle, combined with a Generalized Inverse Beamforming (GIBF) technique, offers the possibility to resolve complex and partially correlated sound sources distributions.

Despite very promising, this approach appears still to be optimized and the influence of a number of potentially influent parameters is to be understood. In this paper a developed GIBF algorithm is combined with a PCA and firstly tested on a simulated problem, then applied on gradually more complex real cases. A sensitivity analysis on some relevant parameters is carried out in order to evaluate the robustness of the developed algorithm and the effectiveness of the used PCA.

Keywords Beamforming • Inverse beamforming • Sound source identification • Principal component analysis • Array methods

List of Acronyms

PCA   Principal Component Analysis
GIBF   Generalized Inverse Beamforming
SVD   Singular Values Decomposition
MAC   Modal Assurance Criterion
CSM   Cross-Spectral Matrix
APS   Auto Power Spectrum
GCV   Generalized Cross-Validation function

5.1 Introduction

The use of Generalized Inverse Beamforming (GIBF), offers the possibility to resolve complex and partially correlated sound sources distributions if used in combination of a PCA of the acoustic field [1]. This makes it particularly suitable in problems of sound source localization where many causes of noise, uncorrelated each other, are active at the same time [2, 3]. This for several reasons: first of all an inverse approach allows defining the most appropriate radiation model [4, 5] for the case in study, allowing also to quantify the strength of the noise sources active in the field; moreover the accuracy in localizing point as well as distributed noise sources is rather constant in frequency.

These undoubted advantages justify the interest in such methodologies, despite a series of drawbacks:

– The inverse formulation leads most of the times to ill-posed problems requiring an effective regularization strategy.
– The decomposition of the acoustic field in uncorrelated sources by means of PCA may be not always ideal.

C. Colangeli (✉) • K. Janssens
Siemens Industry Software NV, Interleuvenlaan 68, 3001 Leuven, Belgium
e-mail: claudio.colangeli@siemens.com

P. Chiariotti
Università Politecnica delle Marche, Via Brecce Bianche 1, 60131 Ancona, Italy
e-mail: p.chiariotti@univpm.it

The influence of such variables on the performances of the technique is still to be deepened. In order to do so, the proposed formulation of GIBF is tested through a sensitivity analysis. A set of optimal values for such parameters will be proposed as well as some guidelines to be used in the application of the method.

5.2 PCA for Uncorrelated Noise Sources Separation

Considering, as in Fig. 5.1, two uncorrelated sources $s_1(t)$ and $s_2(t)$ whose spectra are $S_1(\omega)$, $S_2(\omega)$, and two microphones m_1 and m_2 receiving the abovementioned sources: $P_1(\omega)$ and $P_2(\omega)$, the CSM (C_M) between the signals at the microphones of such a problem is given by the Eq. (5.2).

$$\begin{pmatrix} P_1 \\ P_2 \end{pmatrix} = \begin{bmatrix} G_{11} & G_{21} \\ G_{12} & G_{22} \end{bmatrix} \begin{pmatrix} S_1 \\ S_2 \end{pmatrix} \tag{5.1}$$

$$C_M = \begin{bmatrix} (S_1 G_{11} + S_2 G_{21}) (S_1 G_{11} + S_2 G_{21})^* & (S_1 G_{11} + S_2 G_{21}) (S_1 G_{12} + S_2 G_{22})^* \\ (S_1 G_{12} + S_2 G_{22}) (S_1 G_{11} + S_2 G_{21})^* & (S_1 G_{12} + S_2 G_{22}) (S_1 G_{12} + S_2 G_{22})^* \end{bmatrix} \tag{5.2}$$

Assuming uncorrelated sources we have $i \neq j \Rightarrow S_i S_j^* = 0$. Moreover: $G_{kl} G_{mn}^* = 1 \iff k = m \wedge l = n$. So:

$$
\begin{aligned}
C_M &= \begin{bmatrix} S_1{}^2 + S_2{}^2 & S_1{}^2 \left(G_{11} G_{12}^* \right) + S_2{}^2 \left(G_{21} G_{22}^* \right) \\ S_1{}^2 \left(G_{12} G_{11}^* \right) + S_2{}^2 \left(G_{22} G_{21}^* \right) & S_1{}^2 + S_2{}^2 \end{bmatrix} \\
&= S_1{}^2 \begin{bmatrix} 1 & G_{11} G_{12}^* \\ G_{12} G_{11}^* & 1 \end{bmatrix} + S_2{}^2 \begin{bmatrix} 1 & G_{21} G_{22}^* \\ G_{22} G_{21}^* & 1 \end{bmatrix}
\end{aligned} \tag{5.2.1}
$$

The CSM, is by definition Hermitian, so its eigenvalue decomposition can be obtained in the form (5.3):

$$C_M = E S E^\dagger \tag{5.3}$$

$$E = \begin{bmatrix} G_{11} & G_{21} \\ G_{12} & G_{22} \end{bmatrix} \qquad S = \begin{bmatrix} S_1{}^2 & 0 \\ 0 & S_2{}^2 \end{bmatrix} \tag{5.4}$$

Comparing the Eq. (5.3) and the (5.2.1), the matrices E and S are obtained in Eq. (5.4) showing that the APS of the uncorrelated sources active in the field are eigenvalues for the CSM (see also [2]) and the corresponding eigenvectors depend on their radiation model. This interesting result will be combined with GIBF using the just described PCA to:

– Ascertain the number of uncorrelated sources active in the field.
– Retrieve their strength by means of their corresponding eigenvalue of the CSM.
– Filter out the background noise by discarding the lowest eigenvalues of CSM.
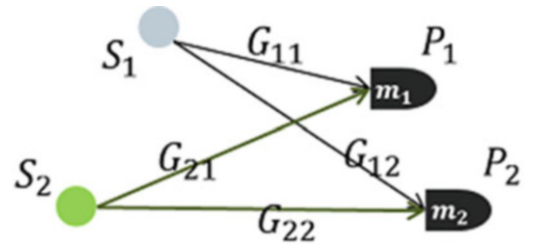
Fig. 5.1 Sources (S_1 and S_2) radiation towards microphones (P_1 and P_2)

5.3   Generalized Inverse Beamforming Formulation

It is proposed a formulation of GIBF for processing phased microphones array measurements aiming at identifying (localization and quantification) the noise sources in an acoustic field. The idea is to reconstruct the measured acoustic field through the superimposition of a distribution of ideal sources disposed in a so-called target grid.

Sources distribution :

$$a_i = \begin{bmatrix} \hat{a}_1 & \dots & \hat{a}_N \end{bmatrix}^T \tag{5.5}$$

Receiver distribution :

$$v_i = \begin{bmatrix} \hat{v}_1 & \dots & \hat{v}_M \end{bmatrix}^T \tag{5.6}$$

Radiation matrix :

$$\{A\}_{m,n} = \frac{e^{-ikr_{mn}}}{4\pi r_{mn}} \tag{5.7}$$

r_{mn} is the distance between the mth of the M microphones and the nth of the N target grid points.

What demonstrated in Sect. 5.2 is here exploited for decomposing the acoustic field at the microphones position in uncorrelated sources distributions through the SVD of the CSM. Considering the Eq. (5.3), this is done as follows:

$$V = \begin{bmatrix} v_1 & \dots & v_l \end{bmatrix} = \sqrt{S} E \tag{5.8}$$

$$Aa = V \tag{5.9}$$

With: $a = [a_1, \dots, a_i, \dots, a_l] \in \mathbb{C}^{N \times l}$, $V \in \mathbb{C}^{M \times l}$, 1: number of not negligible eigenvalues of the CSM.

The unknowns, in (5.9), are the sources distributions a_i related to each eigenmode $\sqrt{s_i} e_i$. So the inverse problem $a = A^{-1} V$ must be solved. For optimizing the solution is adopted the algorithm proposed in [1, 6], formulating per each significant eigenmode v_i the problem $Aa_i = v_i$ and applying the following algorithm:

1. Calculate the initial source vector, a_i by inverting the radiation matrix: $a^0{}_i = (\{A\}_{M*N})^{-1} v_i$
2. Reorder and truncate (10 %) the source vector $a^k{}_i$, discarding the smallest terms
3. Calculate a new source vector: $a^k{}_i = \left(\{A\}_{(0.1^k)M*N} \right)^{-1} v_i$
4. Repeat (2) and (3) until a wanted number of sources is reached.

The Tikhonov's approach will be used for inverting the ill-conditioned radiation matrix. In this paper a robust criterion in the choice of the regularization factor λ is adopted taking advantage of the properties of the SVD of A.

$$A \in \mathbb{C}^{M \times N},$$

$$A = U \Sigma X^\dagger = \sum_{i=1}^{M} u_i \sigma_i x_i{}^\dagger \tag{5.10}$$

$$U \in \mathbb{C}^{M \times M} = \begin{bmatrix} u_1 & \dots & u_M \end{bmatrix}$$

$$\sigma = \text{diag}(\Sigma) = \begin{bmatrix} \sigma_1 & \dots & \sigma_M & 0 & \dots & \sigma_N = 0 \end{bmatrix} \in \mathbb{R}$$

$$X \in \mathbb{C}^{N \times N} = \begin{bmatrix} x_1 & \dots & x_N \end{bmatrix}$$

The candidate regularization factors are chosen among a set of logarithmically distributed regularization parameters between the highest and the lowest non-zero singular value of the radiation matrix A.

Recalling that: $\sigma = \begin{bmatrix} \sigma_1 \ldots \sigma_M \end{bmatrix}$, that $U = \begin{bmatrix} u_1 \ldots u_M \end{bmatrix}$ and $v_i = \begin{bmatrix} v_1 \ldots v_M \end{bmatrix} = \sqrt{s_i} e_i$, the most effective filter factor for regularizing the posed ill-conditioned problem can be selected by minimizing the following quasi-optimality function (5.12) (see reference [7]):

$$f_{cand}(n)_j = \frac{\sigma_j{}^2}{\sigma_j{}^2 + \lambda_{cand}(n)^2} \tag{5.11}$$

$$Q\left(\lambda_{cand}(n)\right) = \sqrt{\sum_{j=1}^{M} \left(1 - f_{cand}(n)_j\right) f_{cand}(n)_j \frac{u_j{}^\dagger v_i}{\sigma_j}} \tag{5.12}$$

$$n = 1, \ldots, Nr$$

$$j = 1, \ldots, M$$

Once λ_k is obtained at each iteration k of the algorithm, the matrix inversion can be obtained per Singular Values or, alternatively, by regularized pseudo-inversion of A:

$$a^k{}_i = \sum_{j=1}^{M} \frac{\sigma_j{}^2}{\sigma_j{}^2 + \lambda_k{}^2} \frac{u_j{}^\dagger v_i}{\sigma_j} x_j \tag{5.13}$$

$$\begin{aligned} \text{M} < \text{N} &\rightarrow a^k{}_i \approx A^\dagger \left(AA^\dagger + \lambda_k{}^2 I\right)^{-1} v_i \\ \text{M} > \text{N} &\rightarrow a^k{}_i \approx \left(A^\dagger A + \lambda_k{}^2 I\right)^{-1} A^\dagger v_i \end{aligned} \tag{5.14}$$

In the presented work Eqs. (5.11), (5.12) and (5.13) are used and compared with other regularization strategies.

5.4   Quantification and Localization of the Sources Strength Active in the GIBF Maps

In this section is presented a novel method for localization and quantification of the sources in a GIBF map. This approach is based on the crucial assumption that the APS of each uncorrelated source active in the field is an eigenvalue for the CSM. Referring to Sect. 5.2 and to Refs. [2, 3], the strength q_m of the source distribution in the GIBF map which is related to the mth eigenvalue of the CSM can be estimated using Eq. (5.15):

$$q_m = \frac{s_m - s_M}{MR_r} \tag{5.15}$$

Where:

s_m: m-th eigenvalue of the CSM
s_M: minimum eigenvalue (noise)

$$R_r = (1/4\pi r)^2$$

r: distance array-source grid
M: Number of microphones

The idea is to find the relation between the estimation of the source strength given by the Eq. (5.15) and the one obtained processing the GIBF map, under the following hypothesis (valid for monopole radiation):

Fig. 5.2 Example of centroids localization in the GIBF map
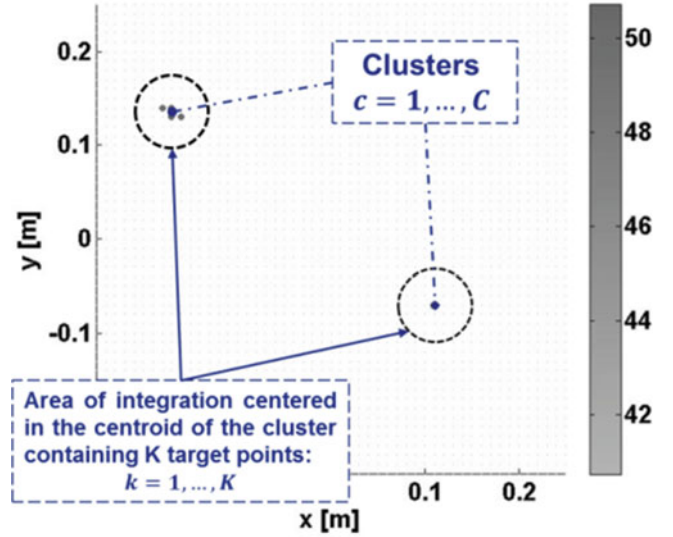
– A source is represented by a cluster of monopoles.
– The monopoles of a cluster have uniform phase (per frequency line) within the cluster.

   The proposed algorithm is summarized below referring to Fig. 5.2:

1. Localization of the C clusters in the GIBF map and their centroids;
2. Consider areas of integration: $cluster(k = 1, \ldots, K)_c$;
3. Sum contributions:

$$P_c = \sum_{k}^{K \epsilon \; cluster_c} a_m \left(cluster(k)_c \right) \tag{5.16}$$

   K: number of the monopoles belonging to the cluster;
4. Comparison with the eigenvalue estimation: $\left| P_c - \sqrt{q_m} \right| < \Delta \; \Rightarrow cluster(k)_c$ is a source distribution.

5.5 Simulated and Real Test Case Scenarios

This sensitivity analysis has been carried out taking as test case a simulated problem of a loudspeakers panel 0.5 m × 0.5 m and an array of 36 microphones placed at a distance of 0.6 m from the panel.

   The same scenario has been replicated in reality using a true loudspeakers panel and the same array geometry used for the simulation. The loudspeakers used in the tests are those identified with number 2 and 4 in Fig. 5.3. From now on these sources will be called Source#1 and Source#2 respectively and considered belonging to an area of tolerance of a radius of 0.05 m. The scenarios presented are summarized in Table 5.1 and Fig. 5.4.

5.6 Sensitivity Analysis

The cross-influence of all the combinations of the following parameters on the GIBF algorithm has been studied:

– Number of averages taken for CSM (AVG): 1,000,667,500,333,100,50,33,10.
– Background noise in data (SNR$_{dB}$): 50,40,30,20,17,10,7,0.

   The signals sample rate is Fs = 20,480 Hz. The beamforming simulation has been carried out in time domain by simulating the delays at the different microphone positions. In all the GIBF calculations has been considered a target grid points distribution equally spaced in the calculation plane with a spatial resolution of 0.01 m. The CSM has been calculated keeping
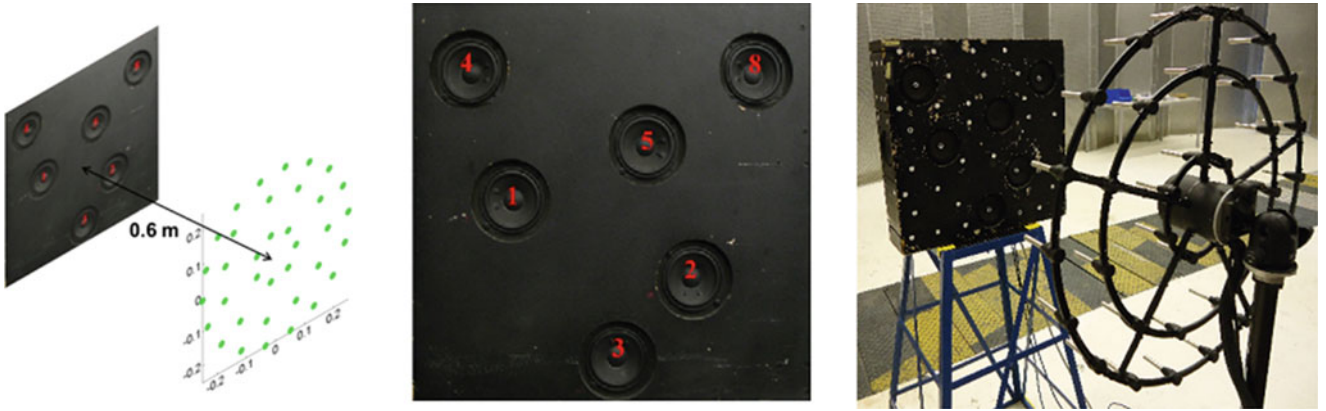
Fig. 5.3 Simulated and real test case on the used loudspeakers panel

Table 5.1 List of the Scenarios presented in this study

Scenario	Source#1	Source#2
a	Random noise	Electric engine noise
b	Random noise	Uncorrelated random noise (same noise level)
c	Random noise	Uncorrelated random noise $\downarrow 10 dB_{SPL}$
d	Random noise	
e	Sine @ 1 kHz	

Fig. 5.4 Sources locations and respective areas of tolerance
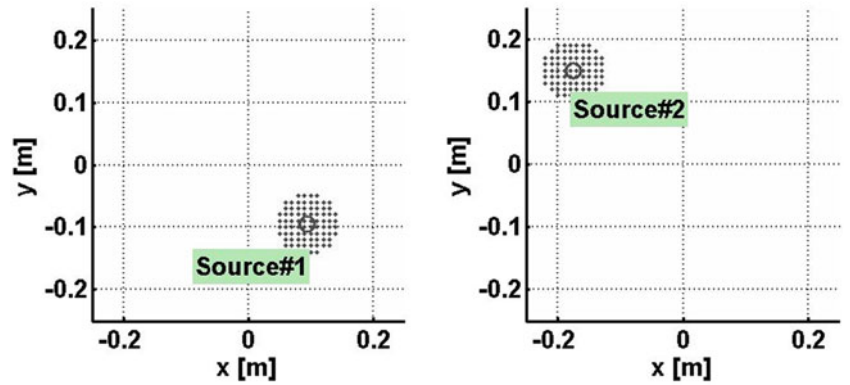
a frequency resolution of 10 Hz. This choice is driven by an analysis on this parameter which is not reported because did not show clearly identifiable trends, but it demonstrated that 10 Hz is a good compromise for strength estimation and calculation time. If not differently specified, the results described below will be presented at a frequency of 1 kHz.

5.6.1 Eigenmodes of the CSM and GIBF Solution for Uncorrelated Sources

Equation (5.4) has shown that the APS of the uncorrelated sources active in the acoustic field are eigenvalues for the CSM. This feature can be exploited for deciding the number and which uncorrelated sources to be used to reconstruct the sound field. This operation will tell information also about the background noise present in the data and if the number of averages taken for computing the CSM is enough for correctly filter it out through the PCA.

According to Eqs. (5.8) and (5.9), since the solution a_i is related to the ith eigenmode of the CSM, its propagation Aa_i towards the array is by definition orthogonal to any other eigenmode of the CSM.

If there are S relevant sources active in the field, it must be:

$$Aa_i, v_j = 0 \ \forall \ j \neq i, \text{ with } j = 1, \ldots, S \tag{5.17}$$
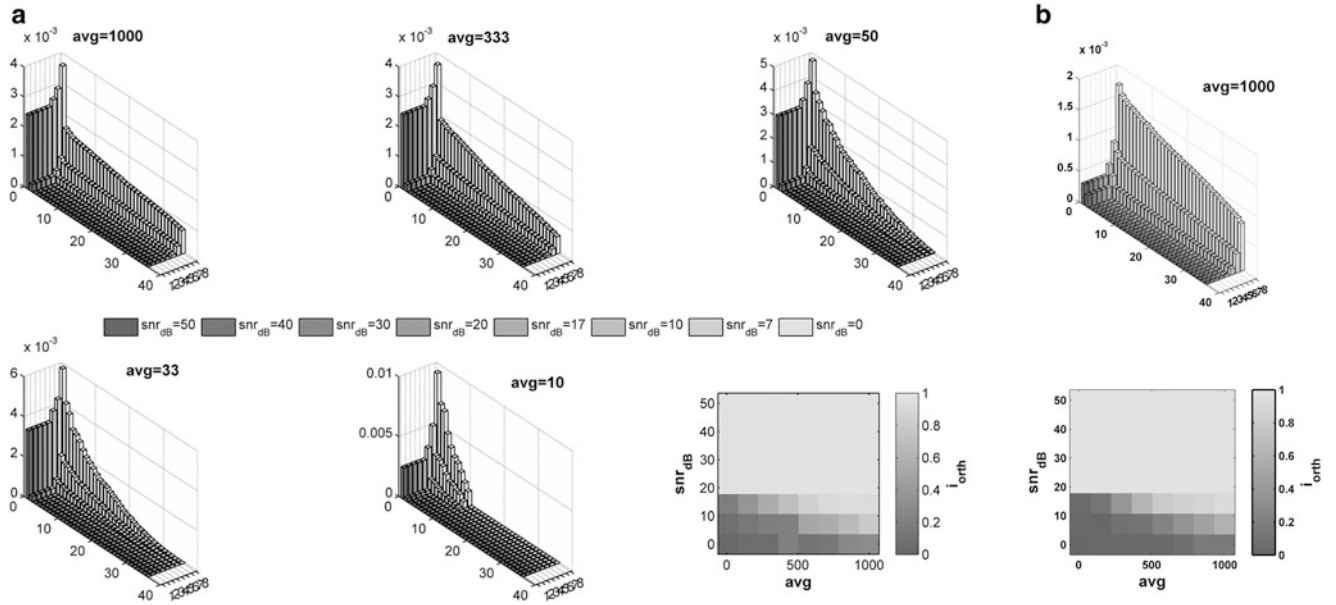
Fig. 5.5 Eigenvalues trend (AVG vs. SNR) and indicator i_{orth} for scenario c (**a**) and scenario b (**b**)

This property can be used for verifying the results. Let us define the following indicator Eq. (5.17) whose trend is shown in Fig. 5.5a bottom right and in Fig. 5.5b bottom.

$$
i, j = 1, \ldots, S \ \rightarrow \ i_{orth} = \det\left(MAC\left\{v_j, Aa_i\right\}\right) = \begin{cases} 1 \rightarrow \text{solutions are orthogonal} \\ < 1 \rightarrow \text{solution are not orthogonal} \end{cases} \tag{5.18}
$$

Figure 5.5 also shows, in two scenarios, the eigenvalues of the CSM ranked in a descended order and grouped per SNR and different number of averages showing that, for GIBF applications, the number of averages should be at least $avg = 10 * M$ (M is the number of microphones), for having the main eigenvalues stable for quantification purposes.

As expected the SNR has a strong influence on the i_{orth} therefore on the solution. Uncorrelated sources with different frequency content permit to tolerate slightly more severe SNR conditions.

5.6.2   Localization, Separation and Quantification

GIBF results for scenario a and scenario b (with real measurements) in the frequency range 800–5,000 Hz and applying $avg = 500$, are shown in Figs. 5.6 and 5.7.

In the case of scenario a (Fig. 5.6), since the frequency content of the two uncorrelated sources is rather different, the identification of the sources is optimal. Figure 5.7 shows a real test case where the two sources APS are very similar producing two effects: difficulty in reconstructing the spectra of the sources (obtained using reference microphones placed in the proximity of the loudspeakers) and presence of numerical ghost images in the GIBF map.

The indicator for evaluating the correct localization of the sources is defined as follows:

$$
i_{loc}(m) = \frac{\sum_{n' \in Source\#1} a_m\left(n'\right) + \sum_{n'' \in Source\#2} a_m\left(n''\right)}{\sum_{n=1}^{N} a_m(n)} \tag{5.19}
$$

The idea is to compare what is inside the areas of tolerance of the two sources with what is all over the GIBF map. In a similar way the quantification can be evaluated. In this case the energy content inside the sources areas is compared with the estimation of the sources strength done through the corresponding eigenvalues. With the notation used in Eqs. (5.15) and (5.16), the strength estimation indicator can be defined as follows:
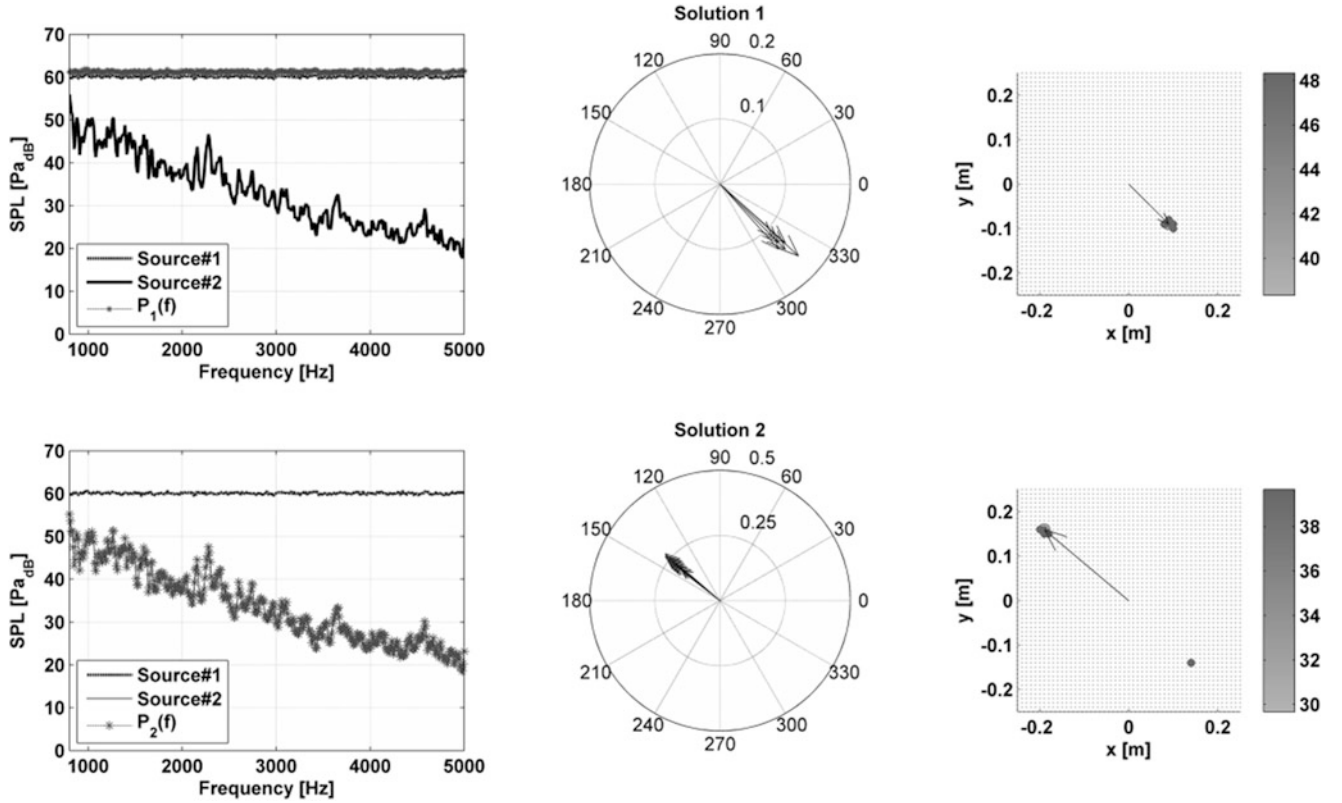
Fig. 5.6 Scenario a. GIBF calculated in the range 800 Hz–5 kHz. Quantification compared with the actual spectra of the sources. Localization shown through a compass plot showing an *arrow* per each spectral line calculated, pointing the retrieved coordinate of the source. An example of beamforming map is shown at 1 kHz

$$i_{str}{}^{(m,1)} = \frac{\sum_{n' \in Source\#1} a_m(n')}{\sqrt{q_m}} \qquad i_{str}{}^{(m,2)} = \frac{\sum_{n'' \in Source\#2} a_m(n'')}{\sqrt{q_m}} \qquad m = 1, \dots, S \qquad (5.20)$$

S is the number of GIBF solutions calculated and it is equal to the number of relevant eigenvalues in the CSM.

Figure 5.8 shows that the sources are correctly localized in both scenarios b and c for SNR >20 dB.

In the scenario c, where one of the uncorrelated sources is stronger than the other, is visible also that the sources are always correctly separated and the quantification. Indeed the conditions of correct separation and quantification described in Eq. (5.21) are fulfilled.

$$\begin{cases} i_{loc} \cong 1 \\ i_{str}{}^{(1,2)} = 0 = i_{str}{}^{(2,1)} \\ i_{str}{}^{(1,1)} = 1 = i_{str}{}^{(2,2)} \end{cases} \qquad (5.21)$$

For scenario b, despite less evident, the trend of the indicators is the same, but with major presence of numerical issues.

5.6.3 Regularization Strategy

In Sect. 5.3 are described the adopted regularization strategy and matrix inversion techniques used so far. Referring to [2], different alternative regularization strategies have been tested and presented here: quasi-optimality, GCV, L-Curve, Lagrange.

Figure 5.9 presents a comparison between the methods in presence of a sinusoidal source at 1 kHz and 1 Pa amplitude placed at the coordinate: [0.095 m −0.095 m] in the shown maps (scenario e). The most effective are the quasi-optimality and GCV functions. The L-Curve still allows localizing the source with a less clear pattern.

Fig. 5.7 Sources spectra calculated with GIBF and compared with reference microphones spectra in a real test case. Example of localization maps without CTC (**a**)
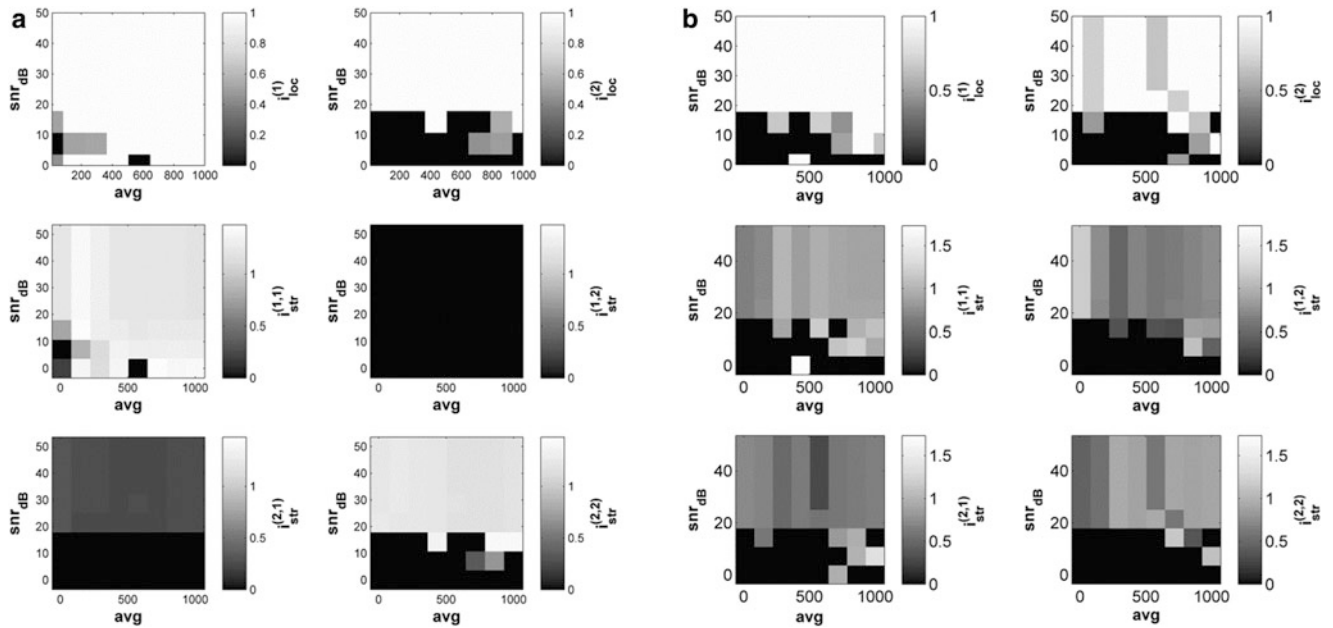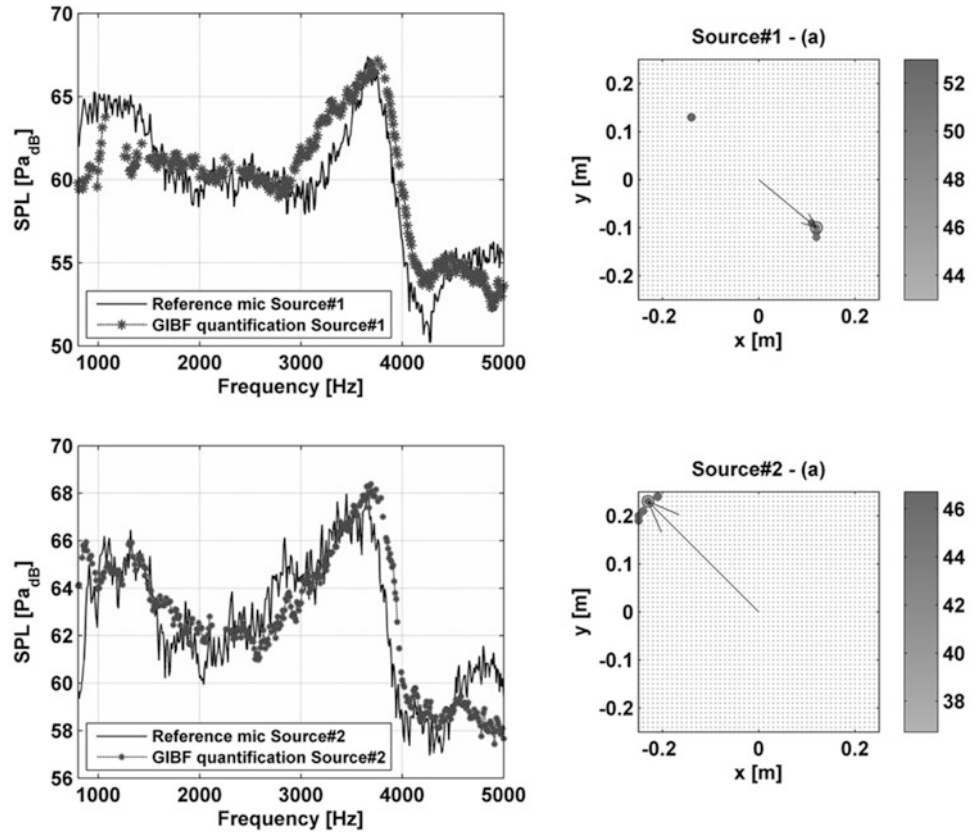

Fig. 5.8 i_{loc} and i_{str} for scenario c (**a**) and for scenario b (**b**). AVG versus SNR

Figure 5.10 shows the trend of the chosen regularization factor during the iterative process of the GIBF algorithm in the four cases. Quasi-optimality and GCV functions yield a similar regularization factor after the first iterations.

The strength of the source is 90 dB. The strength estimation using the different regularization strategies is shown in Table 5.2. The use of Eq. (5.14) instead of Eq. (5.13) has also demonstrated the same trend.
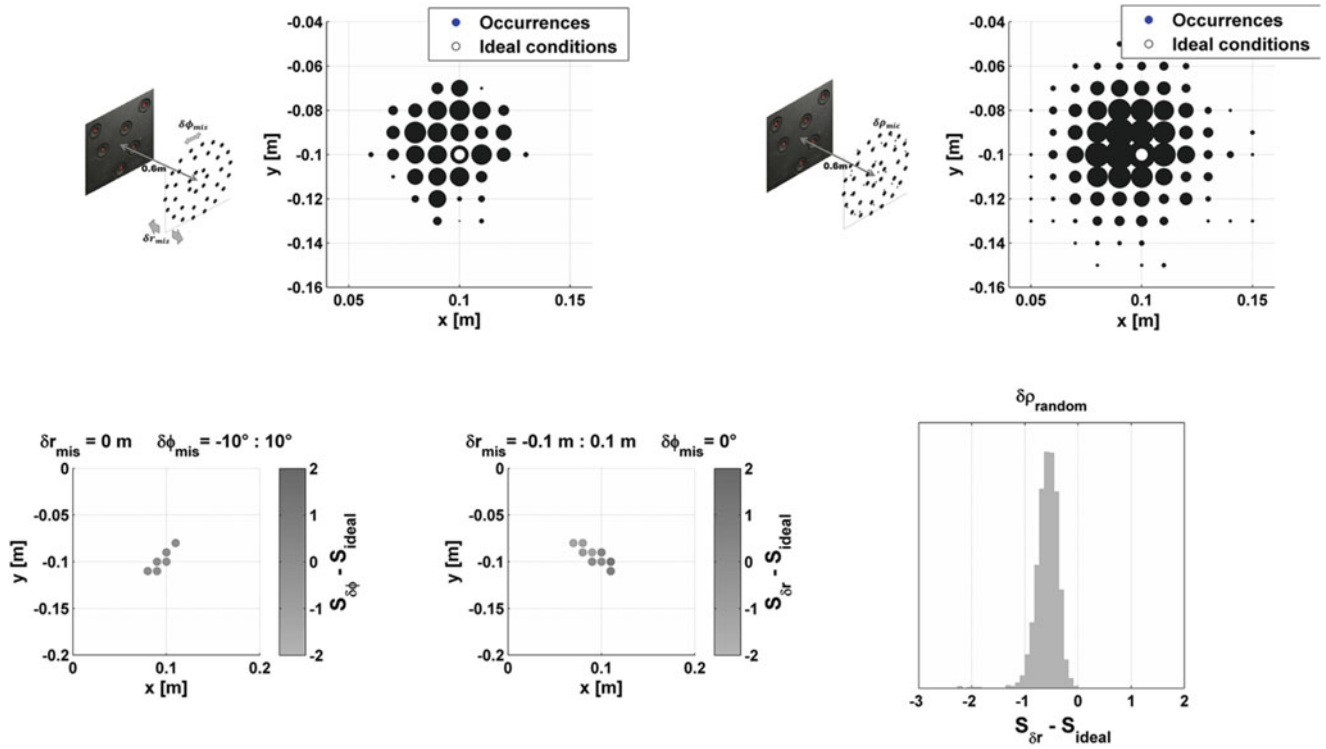
Fig. 5.9 GIBF with different
regularization strategies using Eq.
(5.13) for matrix inversion
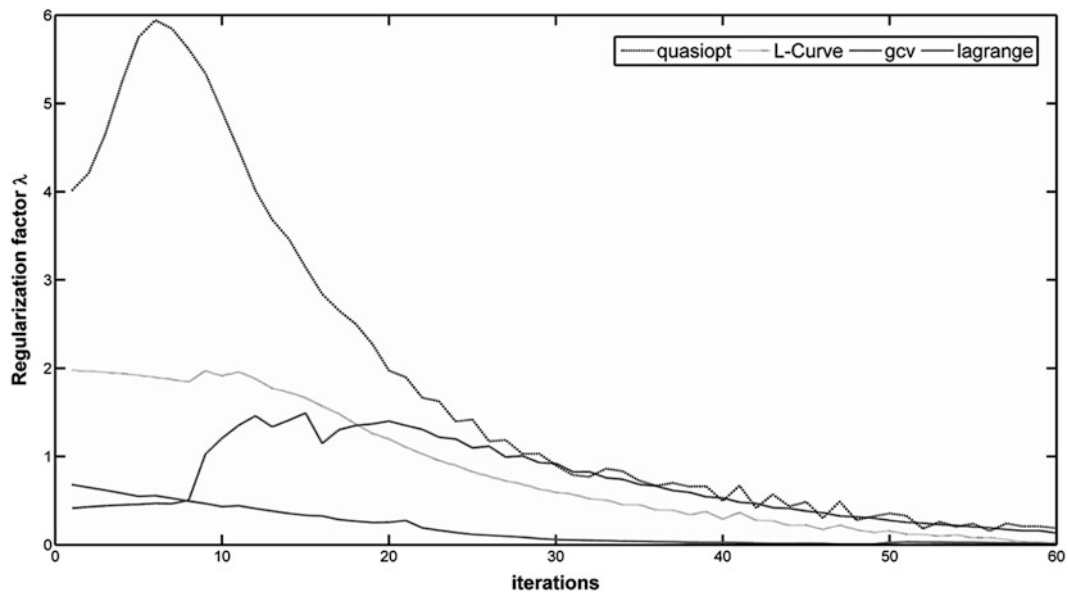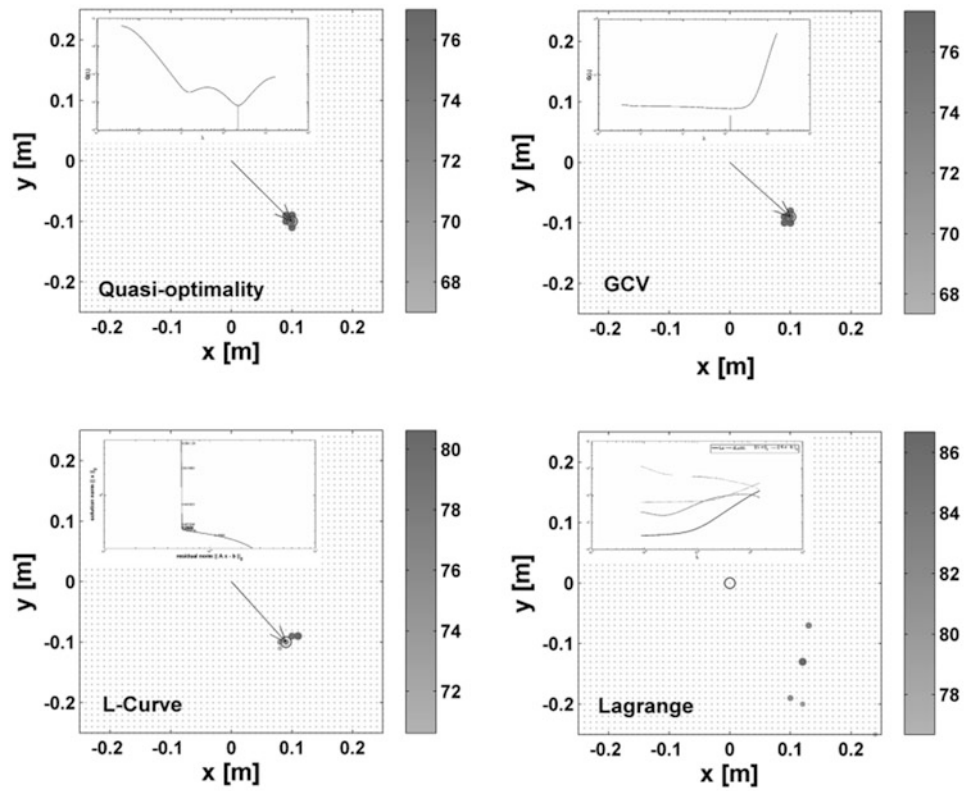
Fig. 5.10 Trend of regularization factor during GIBF iterations

Table 5.2 Strength estimation
using GIBF with different
regularization strategies

1. Quasi-opt	**2.** GCV	**3.** L-curve	**4.** Lagrange
90.8 dB	**90.9 dB**	**91 dB**	**/**

Fig. 5.11 GIBF with wrong positioning of the array (*top-left* and *bottom-left*) and GIBF with wrong positioning of microphones within the array (*top-left* and *bottom-left*)

5.6.4 Influence of Wrong Positioning of the Array and Its Microphones

The robustness of the algorithm to wrong specifications of the geometry has been tested by simulating the most common errors: wrong positioning of the array in the space, wrong positioning of the microphones within the array. In the first analysis the array error in positioning is made varying in the range: $r_{ideal} + \delta r_{mis} = 0.6m \pm 0.1m$ with a 0.01 m step for the distance to the target grid and $\Phi_{ideal} + \delta\Phi_{mis} = 0° \pm 10°$ with a step of 0.1 ° for the error in angle positioning. In the second case the position of each microphone is made randomly varying within a sphere of radius$\delta\rho_{mic} = 0.01$ m centered at the microphone ideal position The size of the dots in the maps in Fig. 5.11 is proportional to the number of occurrences in which the source has been localized in that position. In both analyses the localization error is within an area of about 0.05 m radius. The color of the dots in the graphs at the bottom-left side of Fig. 5.11 is proportional to the difference of the obtained source strength and the one in the ideal position (S_{ideal}). The quantification error is almost not present in the case of angle error, while, as expected, it is proportional to the distance error of the array from the target in the second case. Regarding the random case (Fig. 5.11 bottom-right), in the majority of the cases the source strength is slightly underestimated ($S_\delta - S_{ideal}$ is presented in dB).

5.7 Conclusions

The sensitivity analysis allowed better understanding the influence of most of the relevant parameters in the performances of the formulated GIBF combined with the PCA of the CSM. The main results can be summarized as follows:

– Computing the CSM taking a sufficient number of averages is crucial for correct source quantification and separation. A suitable rule of thumb is taking at least 10*M averages with M sensors in the array. Even though, if the uncorrelated sources spectra are similar, the separation may be not optimal.
– The localization, quantification and separation performances of GIBF are similarly influenced by the presence of background noise in the array measurements. A reasonable threshold is: $SNR \geq 20dB$.

- The conducted analyses on frequency resolution for calculating the CSM didn't show a clear trend, nevertheless 10 Hz resulted to be a good compromise for correctly reconstruct the spectra of the sources.
- The regularization strategy adopted for solving the inverse problem dramatically influences the results and it is crucial, for GIBF, to select the optimal regularization factor at each step of the iterative process. The analysis demonstrated that good options are the so-called quasi-optimality function or GCV function.
- A wrong positioning of the array, or of some microphones within it, introduces errors limited in an area of a 0.05 m radius for localization and a possible wrong estimation of the source within a $\pm 2dB$ range.

What shown in this analysis demonstrates the applicability of GIBF combined with PCA of the CSM for resolving complex acoustic fields, in presence of multiple uncorrelated sources, also with strong background noise. This makes it suitable for applications where these features are needed such as automotive applications, interior beamforming and aeroacoustics.

References

1. Suzuki T (2008) Generalized inverse beamforming algorithm resolving coherent/incoherent, distributed and multipole sources. In: 14th AIAA/CEAS aeroacoustics conference (29th AIAA aeroacoustics conference), Vancouver, 5–7 May 2008
2. Muller TJ (2002) Aeroacoustic measurements. Springer, Berlin
3. Zavala P (2012) Aeroacoustic source and moving source identification. PhD thesis, Faculty of Mech. Eng., University of Campinas, Sao Paulo
4. Dougherty RP (2011) Improved generalized inverse beamforming for jet noise. In: 17th AIAA/CEAS aeroacoustics conference, AIAA 2011–2769
5. Zavala P, De Roeck W, Janssens K, Arruda JRF, Sas P, Desmet W (2010) Monopole and dipole identification using generalized inverse beamforming. In: 16th AIAA/CEAS aeroacoustics conference, Stockholm, Sweden
6. Zavala P, De Roeck W, Janssens K, Arruda JRF, Sas P, Desmet W (2011) Generalized inverse beamforming with optimized regularization strategy. Mech Syst Signal Process 25:928–939
7. Hansen PC (1994) Regularization tools: a matlab package for analysis and solution of discrete ill-posed problems. Num Algorithms 6:1–35